A differential lithium isotope effect on the formation of amorphous calcium phosphate from solution

Joshua S. Straub,[1] Manisha L. Patel,[1] Mesopotamia Nowotarski[2], Lokeswara Rao[2], Mark E. Turiansky[3], Matthew P.A. Fisher[1*], Matthew E. Helgeson[4*]

[1]Department of Physics, University of California, Santa Barbara,
[2]Department of Chemistry, University of California, Santa Barbara,
[3]Department of Materials, University of California, Santa Barbara,
[4]Department of Chemical Engineering, University of California, Santa Barbara,

[*]Correspondence should be addressed to: helgeson@ucsb.edu and mpaf@ucsb.edu

Differential isotope effects are an emerging tool for discovering possible non-trivial quantum mechanical effects within biological systems. However, it is often nearly impossible to elucidate the exact mechanisms by which a biological isotope effect manifests due to the complexity of these systems. As such, one proposed *in vitro* system of study for a quantum isotope effect is calcium phosphate growth, where symmetric calcium phosphate pre-nucleation species, known as Posner molecules, have been theorized to have phosphorus nuclear spin dependent self-binding rates, which could be differently modulated by doping with stable lithium isotopes. Here, we present *in vitro* evidence for such a differential lithium isotope effect on the formation and growth of amorphous calcium phosphate from solution under certain conditions. Experiments confirm that lithium incorporates into amorphous calcium phosphate,

with ^{7}Li found to promote a greater abundance of observable calcium phosphate particles than ^{6}Li under identical solution preparations. These *in vitro* results offer a potential explanation for *in vivo* biological studies that have shown differential lithium isotope effects. Given the importance of calcium phosphate in biological systems – ranging from mitochondrial signaling pathways to key biomineralization processes, as well as the proposed role of Posner molecules as a 'neural qutrit' – these results present an important step in understanding calcium phosphate nucleation as well as the potential role of calcium phosphate for quantum biology and processing.

Introduction

Over the past decade, there has been growing interest in the area of "quantum biology," where quantum mechanics is theorized to be non-trivially functional in a variety of biological systems. Evidence of quantum biological effects exists in a number of systems including proton tunneling in proteins (*1, 2*), olfaction (*3*), photosynthesis (*4–6*), and magnetoreception in birds (*7–10*). However, experimentally confirming or discovering cases of quantum biological effects is a significant challenge, as the warm, crowded environments found in biology are juxtaposed to the cold, isolated environments favorable for discovering and understanding quantum mechanical behavior. One area of interest within quantum biology is spin-based effects, ranging from singlet-triplet conversion in electron spin pairs to nuclear spin information storage (*4,7,11*). Differential isotope effects offer a useful strategy for identifying spin-mediated cases of quantum biology, as the isotopes can have different spin-spin interactions but similar chemical interactions. Recently, a number of biological isotope effects have been discovered which cannot be readily explained by the classical mass-based kinetic isotope effect, including lithium isotope effects on mothering behavior (*12*) and the suppression of mania (*13*) in rats, a xenon isotope

effect on xenon's anesthetic properties in mice (*14*), and recently, a lithium isotope effect on mitochondrial calcium sequestration (*15*). However, due to the complex nature of biological systems, it is almost impossible to definitively place the origins of these isotope effects. Recently, experimental tests of Li isotope effects on key neuronal and enzymatic activities found no distinguishable differences (*16*) that link the observed effects to differential uptake into cells. While the radical pair mechanism has been proposed for both xenon anesthesia and lithium mania suppression (*17, 18*), such modeling efforts are speculative in that they fail to link the spin dynamics to any biological function that would impact the observed behavior. As a result, to build a greater understanding of quantum effects in biological systems, it is important to find *in vitro* systems that demonstrate such non-classical isotope effects so that these quantum effects can be investigated in a systematic manner.

Given the prevalence of apparent lithium isotope effects across a range of biological functions, one broad context to search for such a system considers the formation and growth of calcium phosphate. Calcium phosphate mineralization is important in a wide range of biological contexts, including the formation of hydroxyapatite in teeth and bone (*19, 20*), and in mitochondrial pathways, where amorphous calcium phosphate granules act as biological stores of calcium and phosphate ions (*21, 22*). Lithium has also been proposed to incorporate into calcium phosphate nanoclusters and impact their binding dynamics in an isotope-dependent manner (*11, 23, 24*). Moreover, in medicine, lithium has been implicated in the decalcification of teeth as an unwanted side-effect of lithium-based treatments (*25*), suggesting that lithium may affect the growth and/or stability of calcium phosphate. Thus, the calcium-phosphate-lithium system provides an *in vitro* model with interesting potential for elucidation of possible quantum effects in biological systems.

Recent advances in our understanding of the early stages of calcium phosphate mineralization from solution have confirmed the existence of prenucleation species which provide a novel

route of nucleation and growth (*26–28*). While the exact stoichiometry and structure of these calcium phosphate prenucleation species are still unknown, the two primary proposals are: 1) some form of ionic calcium triphosphate (such as $[Ca(H_2PO_4)_{1.04})(HPO_4)_{1.76}]^{2.56-}$) (*27, 29*), and 2) the Posner molecule ($Ca_9(PO_4)_6$) (*26, 30, 31*). It is also conceivable that these two proposed prenucleation species can exist in equilibrium. The latest understanding of calcium phosphate (ACP) nucleation and aggregation based on these prenucleation species is shown in Figure 1 (*26, 27, 32–35*). Before calcium phosphate nucleation, phosphate ions are in exchange with phosphate assemblies, liquid-like clusters of phosphates that form in aqueous solution (*34*) (stage I). Solution conditions such as ion concentration, temperature, and pH then encourage the formation of prenucleation species from soluble ions (stage II), which nucleate into nanoparticles of amorphous calcium phosphate (ACP) (stage III). These ACP particles then aggregate into larger ACP colloids (*26*) (stage IV) and in time (minutes to hours depending on solution conditions) undergo phase transformation into crystalline hydroxyapatite, the thermodynamically favored phase. (*28, 36*).

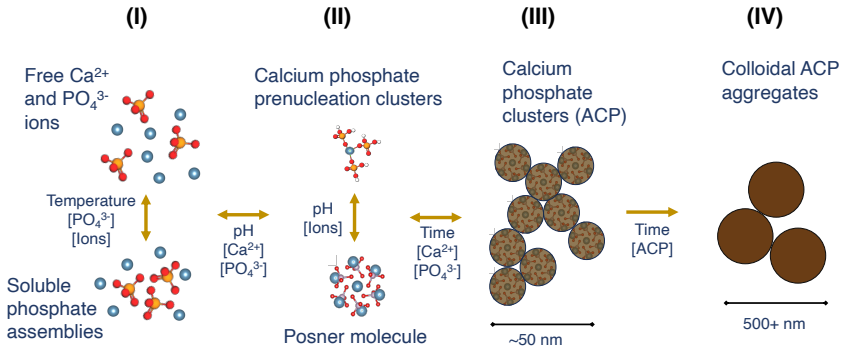

Figure 1: Proposed nucleation and growth pathway for the formation of amorphous calcium phosphate (ACP), showing four proposed stages and the transitions between them. Soluble calcium and phosphate ions (I) initially form prenucleation nanoclusters (II), which then rapidly form calcium phosphate clusters at 50-100 nm in diameter (III). These ACP clusters then aggregate into larger colloidal strcutures at several hundred nanometers in size (IV)). Over time, these metastable ACP aggregates undergo phase transformation to hydroxyapatite.

Within the field of quantum biology, the Posner molecule is of keen interest because of its

putative role in the Posner-mediated Quantum Brain theory (*11, 24*). This theory proposes that the Posner molecule could function as a biological qutrit in a quantum information network that operates alongside a classical biochemical information network in the mammalian brain. Within the framework of this theory, it is posited that one might observe a differential lithium isotope effect on the aggregation of Posner molecules (*24*). Previous density functional theory calculations revealed energetic favorability for two Li-ions to replace the central calcium ion in a Posner molecule (*23*). In such a case, an isotope effect could arise from different couplings between the spin of the two lithium isotopes, ^{6}Li and ^{7}Li, and the ^{31}P spin states within the Posner molecules. Since the collective ^{31}P spin states are proposed to be linked to binding rates of Posner molecules (*23, 24*), such an isotope effect may manifest on larger scales by altering the aggregation of Posner molecules into larger calcium phosphate species. In biologically relevant conditions, it would be expected that the meta-stable phase ACP – sometimes described as a "glass" of Posner molecules (*30, 37, 38*) – would be formed by such initial aggregation events, and thus ACP growth could display isotope-dependent kinetics. Given that ^{6}Li and ^{7}Li have nearly identical electronic states, and thus chemistries, and that their diffusion rate in water differs by only 0.6% (*39*), any observable lithium isotope effect on ACP growth would be classically unexpected by the kinetic isotope effect.

Here, we present results that show a measurable differential lithium isotope effect on the *in vitro* formation of ACP in aqueous solutions that are mildly supersaturated with respect to calcium phosphate. Dynamic light scattering measurements of ACP growth in the presence of ^{6}Li and ^{7}Li salts at biologically relevant pH and temperature reveal that, while the size of ACP particles is insensitive to isotope, the concentration of large ACP particles is enriched in the presence of ^{7}Li relative to ^{6}Li. ^{31}P nuclear magnetic resonance (NMR) and mass spectrometry directly confirm lithium incorporation into ACP and show significant Li-P spin coupling. Given the biological importance of calcium and phosphate regulation, in several established biological

processes as well as the Quantum Brain theory, these results could have wide implications for the interpretation of the milieu of differential lithium isotope effects that have been previously observed.

Dynamic light scattering shows differential lithium isotope effect

Dynamic light scattering (DLS) allows for the measurement of particle sizes in solution, ranging from 1 nm to several microns in diameter, and has previously been used to measure calcium phosphate structures both at prenucleation stages (Fig. 1, II) (*31, 40*) and of larger colloidal structures (Fig. 1, III and IV). (*41, 42*) Here, we used DLS to monitor the size and scattering intensity of calcium phosphate in solutions promoting ACP formation during the first 5 minutes of growth, as monitored in 10 second intervals. A schematic for the preparation and measurement of these solutions is shown in Fig. S1. Solutions were prepared with 250 mM LiCl (either 95% ^{6}Li or 99% ^{7}Li), 2 mM sodium phosphate, and 5 mM $CaCl_2$ at pHs of 7-9 (before calcium) and at 37°C, which is a similar composition to previous studies, although these were done at 25 °C. These specific conditions were chosen due to their biological relevance to the mitochondrial matrix (noting that the pH drops after calcium addition to the 7-8 range), given the mitochondria's importance in buffering intracellular calcium via storage in amorphous calcium phosphate (*21, 22*), and as a potential location of Posner molecules within the Quantum Brain theory.

Prior to calcium addition, the solutions were filtered using 0.2 μm cellulose acetate syringe filters and measured for 120 seconds in DLS to confirm the absence of large contaminant particles. After adding calcium, the average sizes and scattering intensities were measured over a 5-minute interval (Fig. 2). At both pH 7.4 and 8.1, the sizes of ACP measured in the presence of the two lithium isotopes were identical. At the lower pH of 7.4, the scattering intensities

are also isotope-independent, but at pH 8.1 the scattering intensity in the presence of ^{7}Li is significantly higher, potentially indicating a lithium isotope dependence on the formation of ACP from solution.

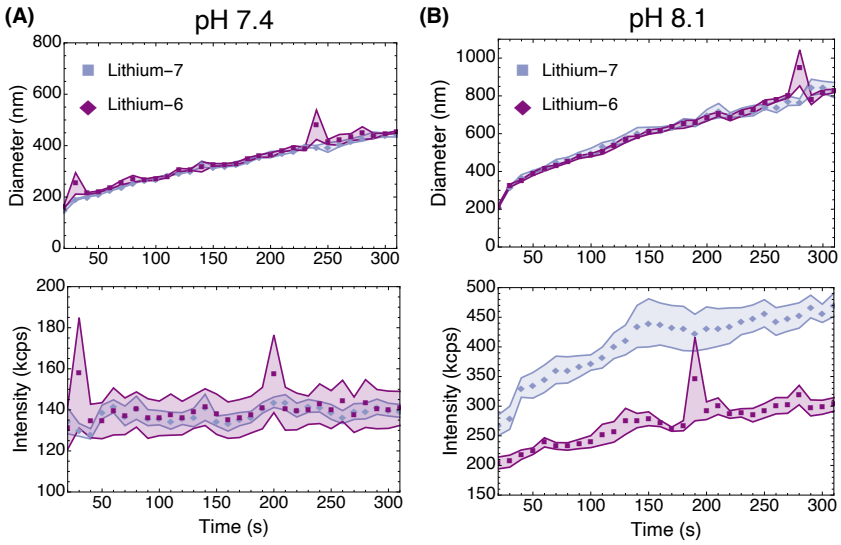

Figure 2: Dynamic scattering results of the first 5 minutes of ACP growth for a system of 5 mM $CaCl_2$, 2 mM $NaPO_4$, and 250 mM LiCl at 37 °C comparing ^{7}Li and ^{6}Li. (A) At pH 7.4, the sizes of calcium phosphate particles and their scattering intensities are the same, indicating no isotopic difference. (B) At pH 8.1, the sizes of calcium phosphate are the same, but the ^{7}Li solution shows greater scattering intensity, indicating a higher particle abundance of structures at large sizes. Each trace is the average result over 5 separate trials, with bands indicating the standard error of the mean. The pH was adjusted to the indicated value before calcium addition using 0.2 M NaOH.

To understand the significance of the different scattering intensities despite the similar average particle sizes between solutions containing the two different lithium isotopes, one can consider how scattering intensity scales with particle size and concentration. Drawing from previous observation (*42*), we consider the wide size dispersity of ACP particles, ranging from prenucleation clusters at the single nanometer scale to larger ACP colloids (Fig. 1 stages II-IV). Mie scattering theory (Fig. S2) shows that, for particle sizes with diameters above the Rayleigh regime (i.e. having diameter $d > \lambda$, where λ is the wavelength of incident light, in this case 532 nm), the scattering intensity I scales approximately as $I \propto d^2$ (*43*), while in the Rayleigh

regime ($d << \lambda$), the scattering intensity drops significantly, with intensity $I \propto d^6$ (*44*). Thus, particles at smaller length scales (1-10 nanometers in diameter) will have negligible contribution to the total scattering intensity compared to the largest ACP particles (at several hundred nanometers in diameter).

Considering this size-intensity relationship, one can then extract information on the distribution of particle sizes within the solutions containing each lithium isotope. Given that the cumulant average size is identical for both isotopes, it appears that the largest particles, which dominate the scattering signal, are forming at the same size in the presence of both isotopes. Therefore, the noted difference in scattering intensity can be attributed predominately to the abundance (concentration) of these largest particles, indicating that the ^{7}Li solution has a more concentrated population of large particles. Given that the total molar concentrations of calcium and phosphate are identical, the ^{6}Li solution must have a more concentrated population of smaller ACP particles, prenucleation species, and/or ionic phosphate and calcium, which contribute minimally to the scattering signal, leading to the observed intensity difference.

To further explore this apparent dependence of ACP formation on lithium isotopes, we explored the solution phase behavior of the LiCl-$NaPO_4$-$CaCl_2$ system to test whether the location of the phase boundaries is isotope-dependent. First, the solid-solution phase boundary was measured in pH and [Ca^{2+}] phase space at fixed [PO_4^{3-}]. 35-minute absorbance measurements at 532 nm identified three distinct regions - a dissolved free ion phase, a metastable colloidal phase, where calcium phosphate particles formed and exhibited time-insensitive absorbance, and an unstable agglomeration phase, where absorbance traces steadily increase and ACP precipitation occurred within 45 minutes (Fig. S4). The results (Fig. 3A) indicate no isotopic dependence on the location of these phase boundaries.

We then monitored ACP growth using DLS at a range of pH within the unstable agglomeration phase to search for the conditions where this isotope effect is present. We find (Fig. 3B)

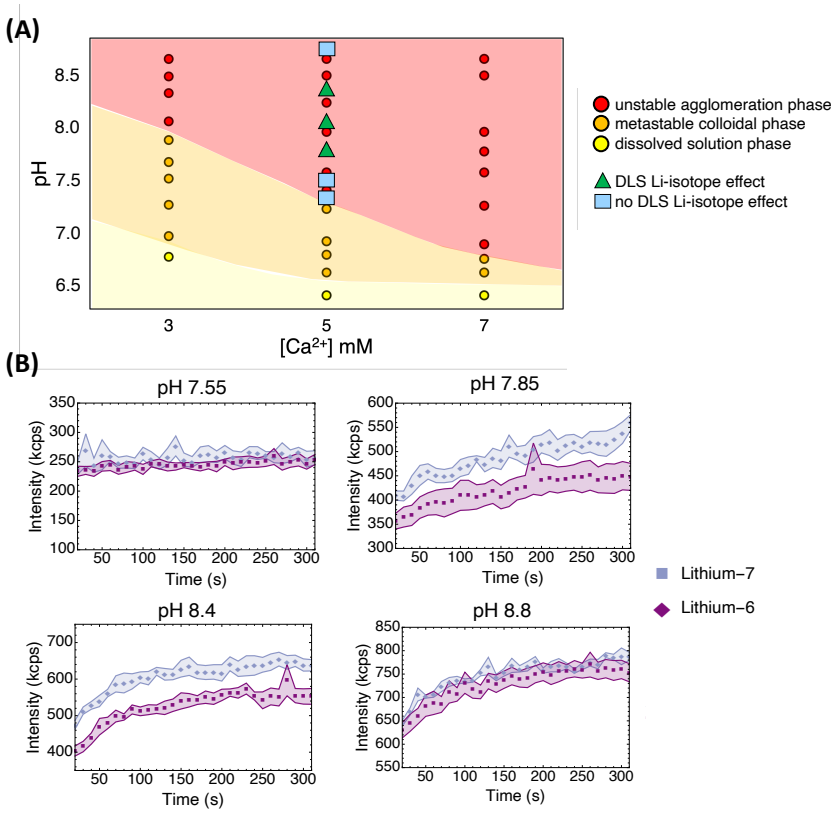

Figure 3: The solution phase behavior of calcium phosphate shows a specific region of active lithium isotope effect. (A) A phase diagram as a function of pH and calcium concentration reveals three distinct regions of ACP growth: 1) dissolved free ions, 2) metastable colloidal aggregates, and 3) unstable agglomeration of clusters. No isotope difference is found in the location of the boundaries between these regions. (B) Exploring pH within the unstable agglomeration phase reveals a distinct pH window where the lithium isotope effect on DLS scattering intensity on ACP growth is observable. All samples had identical sizes from DLS as shown in S3.

that the lithium isotope effect manifests in a specific range of supersaturation, whereas solutions too close to the agglomeration boundary or at too high of a supersaturation show little or no scattering intensity differential. This narrow window indicates that there may be a specific nucleation and growth pathway for ACP formation which shows a differential lithium isotope effect, while other pathways do not allow for this effect.

Lithium acts on early stage calcium-phosphate nucleation

Having established a differential lithium isotope effect in a particular range of compositions *in vitro*, we designed experiments to investigate at what stage in the ACP formation pathway (Fig. 1) this effect manifests. Given that DLS is primarily sensitive to structures at several hundred nanometers in scale, any of the steps leading up to the formation of such large ACP aggregates (stage 4) could be involved in the isotope effect. Therefore, we tested the possibility that a lithium isotope effect could occur at each stage of the ACP growth process.

First, we consider whether stage I, before any calcium phosphate structures have formed, could be differentially impacted. Such an effect could arise, for example, from different local water structuring around atoms of the two lithium isotopes, or due to a direct lithium-phosphate interaction (we assume no significant lithium-calcium interactions given they are both positively charged). As noted, ^{6}Li and ^{7}Li have aqueous diffusion coefficients that differ by $< 0.6\%$ (*39*). This diffusion coefficient is proportional to the hydrodynamic diameter of the ions, which includes the bound water molecules around the ion. Thus, we expect no significant isotopic difference in the local water structuring.

To address the possibility of differential ionic lithium-phosphate interactions, we characterized solutions of lithium and phosphate using ^{31}P NMR before adding calcium. The resulting spectra (Fig. 4A) show nearly identical chemical shift and line width for phosphorus in the presence of ^{6}Li and ^{7}Li, indicating no significant difference in ionic lithium-phosphate chem-

istry. The small observed chemical shift difference of $\sim$0.01 ppm is of the order typically seen for isotopes, given that their different masses will change equilibrium bond length and therefore electron density at the phosphorus nucleus (*45*). We conclude that the observed isotope effect is not likely to manifest during stage I of ACP growth.

To investigate the potential for an isotope effect on later stages of ACP growth, we first established whether lithium is incorporated into the resulting calcium phosphate phase in an isotope-dependent manner. ^{31}P NMR performed after calcium addition indicates a ^{31}P shift in line shift and line width compared to solutions containing no calcium (Fig. 4A), confirming that a new phase of calcium-phosphate forms which we identify as ACP. The ^{31}P signal for ACP in the presence of both lithium isotopes were again similar in line width and position, suggesting that lithium incorporates into the calcium phosphate aggregates in an isotope-independent manner.

The incorporation of lithium into the calcium phosphate phase was confirmed using inductively coupled plasma mass spectrometry (ICP-MS). An ACP powder was synthesized as described in the Materials and Methods section, such that initial calcium phosphate nucleation conditions were identical to those measured in DLS. Therefore, if lithium is incorporated in this synthesized powder, then we would also expect it to be present in the soluble structures that we measure using DLS. ^{31}P and ^{6}Li spin counting experiments verified that this synthesized powder was ACP, and that there was no reprecipitated LiCl in the powder (Fig. S5). ICP-MS traces for ACP powders synthesized in the presence of 250 mM ^{6}LiCl and ^{7}LiCl indicate that both isotopes were incorporated into the resulting phase at $\sim$ 1 wt% (Fig. 4B), with the large error bars resulting from difficulties in ablating the solid powders and mass-dependent transport through the apparatus. Assuming that ACP is $\propto$ 20 wt% water (*46*) and composed of a glass of Posner molecules of stoichiometry $Ca_9(PO_4)_6$, this concentration would correspond to approximately one lithium ion per Posner molecule, indicating that enough lithium may be in-

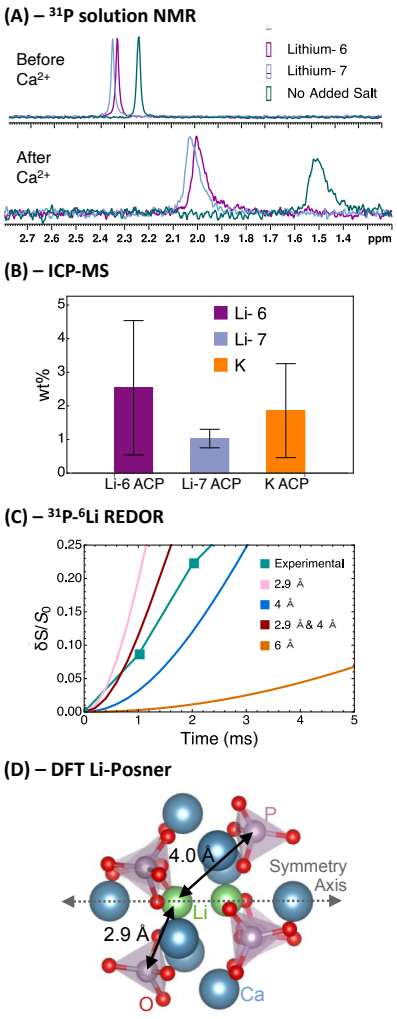

Figure 4: ^{31}P NMR and ICP-MS confirm the incorporation of lithium into ACP phase. (A) ^{31}P NMR on LiCl-$NaPO_4$-$CaCl_2$ solutions shows similar ^{31}P chemical shift in the presence of ^{7}Li and ^{6}Li both before and after the addition of calcium, indicating no isotopic difference in phosphate-lithium interactions and similar incorporation of both lithium isotopes into the ACP phase. (B) ICP-MS results on the incorporation of ^{6}Li, ^{7}Li, and K on ACPs synthesized in the presence of 250 mM ^{6}LiCl, ^{7}LiCl, and KCl. Both lithium isotopes are incorporated similarly into the ACP phase at $\sim$ 1 wt%, with error bars indicating the standard error across 10 independent trials. Potassium is also incorporated at $\propto$ 1 wt%, but given that potassium is 6-7 times as massive as lithium, its incorporation is much less favorable. (C) ssNMR REDOR on ^{31}P-^{6}Li coupling shows lithium-phosphorus distances of $\leq$ 4 Å. A fit with an equal mix of 2.9 Å and 4 Å distances, based on the DFT calculations for the geometry of a Posner molecule with two lithiums replacing the central calcium, shown in (D), shows agreement with the experimental curve.

corporated to have a significant impact on Posner dynamics. Although such "doping" of ACP with lithium has not been reported previously in experiments, previous DFT calculations on Posner molecules indicated an energetic preference for two lithium ions to replace the central calcium ion (*23*), providing a potential explanation for the observed lithium incorporation.

Having established that lithium incorporates into ACP in an isotope *in*dependent manner, we consider whether later stages of ACP growth could be impacted by lithium addition in an isotope-dependent manner. For the growth of calcium phosphate clusters ($\sim$ 100 nm in diameter) into larger aggregates (several hundred nm – several microns), we expect that the colloidal aggregation of ACP particles in aqueous salt solution is dominated by Derjaguin-Landau-Verwey-Overbeek interactions, i.e., an interplay between short-range van der Waals attractions and longer-range electrostatic repulsion (*47*). Since the lithium isotopes have the same charge and electronic structure, neither of these forces should show a strong isotope dependence, so it is unlikely that the lithium isotope effect arises at this stage. We also observe that the calcium phosphate solid-state boundary shows no isotopic dependence (Fig. 3A), in agreement with the DLS results that show that there is no isotopic dependence of ACP size. wW expect the concentration of metastable ACP particles to be primarily determined by the degree of supersaturation of calcium phosphate in solution, and so we infer that there does not appear to be a differential lithium isotope effect on stages III and IV of ACP growth.

Given the above arguments, neither the earliest (ionic) nor latest stages (colloidal aggregation) of ACP growth seem likely to be the source of the observed isotope effect. Therefore, we propose that it is during the formation and aggregation of nanoclusters (stage II) of ACP growth that the differential lithium isotope effect must be operative.

A possible mechanism for a differential isotope effect

To understand a possible mechanism for the lithium isotope effect on calcium phosphate growth, we consider the physical differences between the properties of ^{6}Li and ^{7}Li ions within putative ACP prenucleation species (e.g., Posner molecules). Since the two isotopes of lithium have essentially identical electronic structure, this would presumably rule out any chemical differences in interactions between lithium isotopes, and their nearly identical diffusivities in water indicate similar dynamics in solution. However, the nuclear spin properties of ^{6}Li and ^{7}Li differ significantly. ^{6}Li is a spin-1 nucleus, although due to its small quadrupole moment, it is often considered an "honorary spin-$1/2$" nucleus, with a T_1 relaxation time on the order of minutes in water (*48*). On the other hand, ^{7}Li is a spin-$3/2$ nuclei, with a quadrupole moment two orders of magnitude greater than ^{6}Li, and a T_1 on the order of seconds in water (*48*). Therefore, we expect these two lithium isotopes could have significantly different spin coupling to the ^{31}P nuclei within the Posner molecule, and thus affect their aggregation dynamics, as will be expanded upon later.

To experimentally test whether lithium is proximal enough to phosphorus to have notable spin coupling between the two nuclei, we used the rotational-echo, double-resonance nuclear magnetic resonance (REDOR) sequence on an ACP powder synthesized in the presence of 250 mM ^{6}Li. Briefly, REDOR measure dipolar coupling between two heteronuclear spins, from which an inter-spin distance can be extracted (*49*). For these measurements, ^{6}Li was chosen in the preparation of ACP over ^{7}Li due to its significantly slower relaxation rate, which aids in data acquisition and analysis. However, given that solution NMR and ICP-MS results show similar level of incorporation of ^{6}Li and ^{7}Li into ACP, we expect the results on the ^{6}Li system to also provide insight into the ^{7}Li system.

While REDOR can be difficult to fit to extract precise distances when there is a dispersity

of inter-nuclei distances and multi-spin (≥ 3) effects, the early time REDOR buildup curve can still indicate the strongest dipolar couplings (and thus shortest distances) in the system. The early-time ^{31}P-^{6}Li REDOR curve (Fig. 4C) shows a measurable signal buildup that indicates significant ^{31}P-^{6}Li spin coupling and ^{31}P-^{6}Li distances on the scale of 3-4 Å (the REDOR curve for a 6 Å distance is also shown to illustrate that even slightly farther distances produce large differences in the observed signal). DFT calculations on a Posner molecule with two lithium ions replacing the central calcium ion yield lithium-phosphorus distances of 2.9 Å for three ^{31}P's and 4 Å for the other three ^{31}P's, and a REDOR model based on this distance distribution shows good agreement with the experimentally measured buildup curve. Regardless of specific distances, the close proximity of the two spins indicates a spin-coupling based mechanism for the differential isotope effect could be physically possible. Notably, DFT indicates that this lithium-doped Posner molecule maintains three-fold symmetry within 0.05 Å, the importance of which is expanded upon below.

Colloidal aggregation can be theoretically described as a diffusion-reaction process by which — for the case of pair binding — individual particles encounter one another by diffusive transport and bind through intermolecular and surface forces. In the case of Posner molecules, calculations on the energy landscape for pair binding have found an energetically preferred orientation of pair binding in which Posner molecules have their C_3 axes anti-aligned (*23*). This suggests that there is significant coupling between the rate of pair binding to the orientational dynamics, and thus the relative angular orbital momentum states, of a binding pair of Posner molecules. This provides a potential link between colloidal aggregation and the ^{31}P states of Posner molecules, as follows.

Within the framework of the Quantum Brain theory, the so-called quantum dynamical selection rule posits that the collective ^{31}P spin states within the Posner molecule function as a qutrit with a quantum number defined by the phase factor acquired during a symmetry-preserving

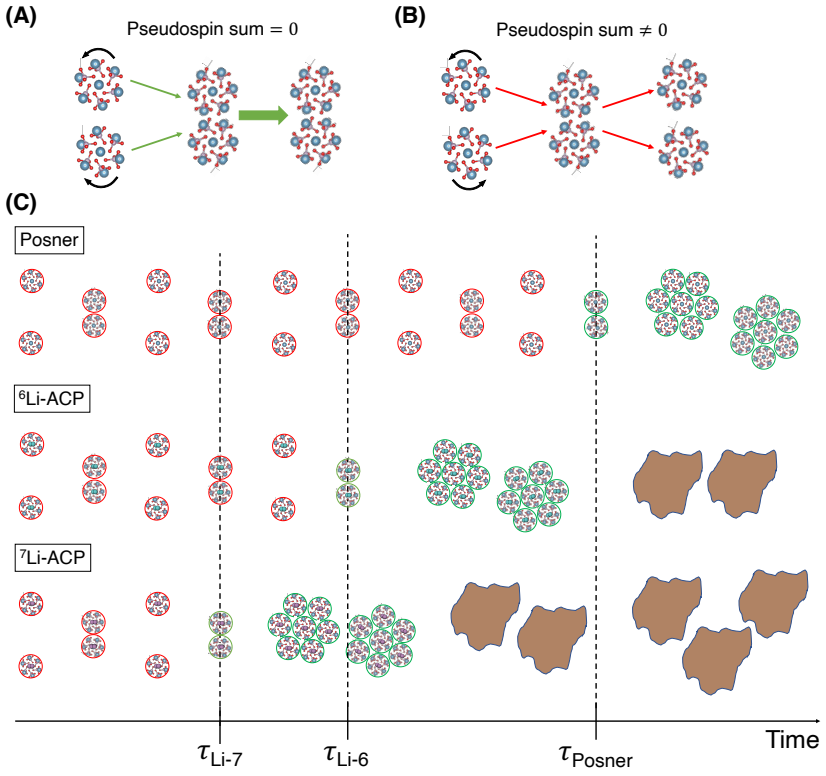

Figure 5: An illustration of a potential mechanism for the impact of pseudospin on Posner molecule pair binding. (A) Two anti-aligned Posner molecules with total pseudospin of 0 are able to access a real wave function that is required for bonding. Black arrows indicate that the pseudospins are opposite in this case. (B) Two anti-aligned Posner molecules with non-zero total pseudospin (black arrows in the same direction) are unable to form a real wave function, thus bond formation cannot occur. (C) The pseudospin coherence time, τ, would be shorter for Li-7 doped Posners compared to Li-6 doped or undoped Posners. After a pseudospin restricted binding attempt, the pseudospin would decohere fastest for Li-7 Posners, allowing them to make a new projective measurement onto pseudospin and bind. These bound pairs can then aggregate into larger ACP clusters, resulting in more clusters at the largest size in the presence of Li-7 as compared to Li-6.

rotation, which we call the "pseudospin." (*24*). Due to the Fermi statistics of the spin-$\frac{1}{2}$ phosphorus nuclei under this rotation, the orbital angular momentum (and rotational dynamics) of the molecule is then constrained by this pseudospin. In this way, only certain spin sectors (that sum to zero) are able to access a real wave function (and stop relative rotation between molecules) which is a requirement to form a chemical bond between pairs of Posner molecules (Fig. 5A,B). In this way, the ^{31}P spin states of the Posner molecules are proposed to impact the apparent chemical reaction rates of Posner molecule pair-binding and, subsequently, downstream aggregation events in the growth of amorphous calcium phosphate. Note that while we focus on the Posner molecule here, quantum dynamical selection would hold for any calcium phosphate nanocluster with a threefold or greater symmetry axis, such as the calcium phosphate dimer that has been proposed to have longer spin coherence times than the Posner (*50*).

This proposal is difficult to test directly because NMR is unable to probe the collective spin state of a molecule, instead measuring an ensemble of spin states across all spins within a given chemical environment. However, we can still consider what measurable consequences the theory would have. These collective spin states will eventually decohere, in a sort of analog to the conventional T_2 relaxation rate for a single spin in NMR, allowing for previously precluded binding to occur. The rate of this decoherence will depend on the coupling of the spins within which the collective state is encoded (here ^{31}P) to the environment (including other spins within the molecule, such as lithium). Therefore, if two isotopes with different spins were to be incorporated into prenucleation species while preserving the molecular symmetry, one might expect the collective spin state lifetime to differ. In such a case, there might be an appreciable difference in pair-binding reaction rates between the two different isotopically doped species. This concept is shown schematically in Fig. 5C, comparing a typically composed Posner molecule with Posner molecules doped with ^{6}Li and ^{7}Li.

While this proposal is still speculative, it is currently difficult to put forward any other

potential explanation for the observed experimental finding. Our ^{31}P NMR, ICP-MS, and phase mapping results rule out ionic interactions, differential incorporation, or solid phase behavior as potential causes for this isotope effect. As such, this highly unusual effect implies the need for an unconventional understanding of calcium phosphate aggregation. Regardless of the exact mechanism behind the observed isotope effect, the discovery of an *in vitro* lithium isotope effect on ACP growth is an important step toward understanding the *in vivo* lithium isotope effects that have been observed in a wide range of biological systems.

Conclusion

We have presented evidence for a differential lithium isotope effect on the *in vitro* formation of amorphous calcium phosphate at biologically relevant conditions. Dynamic light scattering experiments showed that while the size of ACP formed is identical in the presence of ^{6}Li and ^{7}Li, certain conditions promote a measurable difference in scattering intensity that indicates a difference in the abundance of nanoscale ACP clusters. ^{31}P NMR measurements confirm the incorporation of both lithium isotopes into the ACP phase and indicate the presence of Li-P spin couplings, indicating the possibility that the observed isotopic effect may be due to differing nuclear spin interactions between ^{6}Li or ^{7}Li with ^{31}P. The reported isotopic effect could potentially be explained by a quantum-based condition for symmetric pre-nucleation molecular binding, where the spins of the two lithium isotopes differentially impact the probability of Posner binding during early nucleation events.

Our experiments suggest the existence of an *in vitro* differential lithium isotope effect, which has previously only been seen in biological systems. These results offer a potential physical mechanism for previously observed *in vivo* lithium isotope effects, and is consistent with predictions by the Posner molecule-mediated Quantum Brain theory. Given these findings, we propose that additional investigations of differential isotope effects – both for lithium and other

elements – on mineralization processes be undertaken both *in vivo* and *in vitro* to expand our understanding of putative quantum phenomena in both biological and abiotic systems.

Acknowledgements

The authors would like to acknowledge Michel Gingras for a careful reading of the manuscript, as well as Tobias Fromme, Marshall Deline, Songi Han, and Zoya Leonenko for many useful discussions. This work was partially supported by the Heising-Simons Foundation (Award number 2020-2427) and by Ionis Pharmaceuticals (Award number PO 581247). Computational work utilized facilities purchased with funds from the National Science Foundation (CNS-1725797) and administered by the UC Santa Barbara Center for Scientific Computing (CSC). The CSC is supported by the California NanoSystems Institute and the Materials Research Laboratory, a National Science Foundation MRSEC (NSF DMR 2308708). This work also utilized MRL Shared Experimental Facilities supported by the MRSEC Program of the NSF under Award No. DMR 2308708; a member of the NSF-funded Materials Research Facilities Network (www.mrfn.org). This work utilized magnetic resonance instrumentation that was also supported in part by NSF Major Research Instrumentation award, MRI-1920299.

References and Notes

1. P.-O. Löwdin, *Rev. Mod. Phys.* **35**, 724 (1963).

2. A. Kohen, J. P. Klinman, *Chemistry & biology* **6**, R191 (1999).

3. L. Turin, *Chemical Senses* **21**, 773 (1996).

4. C. C. Gradinaru, *et al.*, *Proceedings of the National Academy of Sciences* **98**, 2364 (2001).

5. G. S. Engel, *et al.*, *Nature* **446**, 782 (2007).

6. F. Fassioli, R. Dinshaw, P. C. Arpin, G. D. Scholes, *Journal of The Royal Society Interface* **11**, 20130901 (2014).

7. K. Schulten, C. E. Swenberg, A. Weller, *Zeitschrift fÃŒr Physikalische Chemie* **111**, 1 (1978).

8. W. Wiltschko, R. Wiltschko, *Journal of Comparative Physiology A* **191**, 675 (2005).

9. H. Mouritsen, T. Ritz, *Current Opinion in Neurobiology* **15**, 406 (2005). Sensory systems.

10. C. T. Rodgers, P. J. Hore, *Proceedings of the National Academy of Sciences* **106**, 353 (2009).

11. M. P. A. Fisher, *Annals of Physics* **362**, 593 (2015).

12. J. Sechzer, K. Lieberman, G. Alexander, D. Weidman, P. Stokes, *Biological Psychiatry* **21**, 1258 (1986).

13. A. Ettenberg, *et al.*, *Pharmacology Biochemistry and Behavior* **190**, 172875 (2020).

14. N. Li, *et al.*, *Anesthesiology* **129**, 271 (2018).

15. M. Deline, *et al.*, *Frontiers in Physiology* (2023).

16. J. D. Livingstone, M. J. Gingras, Z. Leonenko, M. A. Beazely, *Biochemistry and Biophysics Reports* **34** (2023).

17. J. Smith, H. Zadeh Haghighi, D. Salahub, C. Simon, *Scientific Reports* **11**, 6287 (2021).

18. H. Zadeh-Haghighi, C. Simon, *Scientific Reports* **11**, 12121 (2021).

19. N. Blumenthal, A. Posner, *Cal. Tis Res.* **13**, 235 (1973).

20. S. V. Dorozhkin, M. Epple, *Angewandte Chemie International Edition* **41**, 3130 (2002).

21. A. L. Lehninger, *Biochemical Journal* **119**, 129 (1970).

22. S. G. Wolf, *et al.*, *Elife* **6**, e29929 (2017).

23. M. W. Swift, C. G. Van de Walle, M. P. A. Fisher, *Physical Chemistry Chemical Physics* **20**, 12373 (2018).

24. M. P. A. Fisher, L. Radzihovsky, *Proceedings of the National Academy of Sciences* **115**, E4551 (2018).

25. C. de P. Eduardo, P. d. F. A. Simões, V. Arana-Chavez, J. Nicolau, V. Gentil, *Special Care in Dentistry* **33**, 91 (2013).

26. A. Dey, *et al.*, *Nature materials* **9**, 1010 (2010).

27. W. J. Habraken, *et al.*, *Nature communications* **4**, 1 (2013).

28. K. He, *et al.*, *Science Advances* **6**, eaaz7524 (2020).

29. E. M. M. Weber, *et al.*, *Analytical Chemistry* **92**, 7666 (2020). PMID: 32378878.

30. F. Betts, A. Posner, *Materials Research Bulletin* **9**, 353 (1974).

31. A. Oyane, K. Onuma, T. Kokubo, A. Ito, *The Journal of Physical Chemistry B* **103**, 8230 (1999).

32. A. L. Boskey, A. S. Posner, *The Journal of Physical Chemistry* **77**, 2313 (1973).

33. F. Grases, M. Zelenková, O. Söhnel, *Urolithiasis* **42**, 9 (2014).

34. J. S. Straub, *et al.*, *Proceedings of the National Academy of Sciences* **120**, e2206765120 (2023).

35. L. Wang, S. Li, E. Ruiz-Agudo, C. V. Putnis, A. Putnis, *CrystEngComm* **14**, 6252 (2012).

36. A. Lotsari, A. K. Rajasekharan, M. Halvarsson, M. Andersson, *Nature Communications* **9**, 4170 (2018).

37. A. S. Posner, F. Betts, *Accounts of Chemical Research* **8**, 273 (1975).

38. G. Mancardi, C. Tamargo, D. Tomasso, N. de Leeuw, *Journal of Materials Chemistry B* **5**, 7274 (2017).

39. P. F. Renshaw, *Biological Psychiatry* **22**, 73 (1987).

40. K. Onuma, *et al.*, *The Journal of Physical Chemistry B* **104**, 10563 (2000).

41. J. R. de Bruyn, *et al.*, *PLOS ONE* **8**, 1 (2013).

42. V. Čadež, *et al.*, *Crystals* **8** (2018).

43. G. Mie, *Annalen der Physik* **331**, 597 (1908).

44. L. Rayleigh, *Proceedings of the Royal Society of London. Series A, Containing Papers of a Mathematical and Physical Character* **94**, 296 (1918).

45. C. J. Jameson, *Isotope Effects on Chemical Shifts and Coupling Constants* (John Wiley Sons, Ltd, 2007).

46. A. S. Posner, N. C. Blumenthal, A. L. Boskey, F. Betts, *Journal of Dental Research* **54**, 88 (1975).

47. J. N. Israelachvili, *Intermolecular and surface forces* (Academic Press London ; San Diego, 1991), second edn.

48. M. Mohammadi, S. Benders, A. Jerschow, *The Journal of Chemical Physics* **153**, 184502 (2020).

49. T. Gullion, *Concepts in Magnetic Resonance* **10**, 277 (1998).

50. S. Agarwal, D. R. Kattnig, C. D. Aiello, A. S. Banerjee, *The Journal of Physical Chemistry Letters* **14**, 2518 (2023).

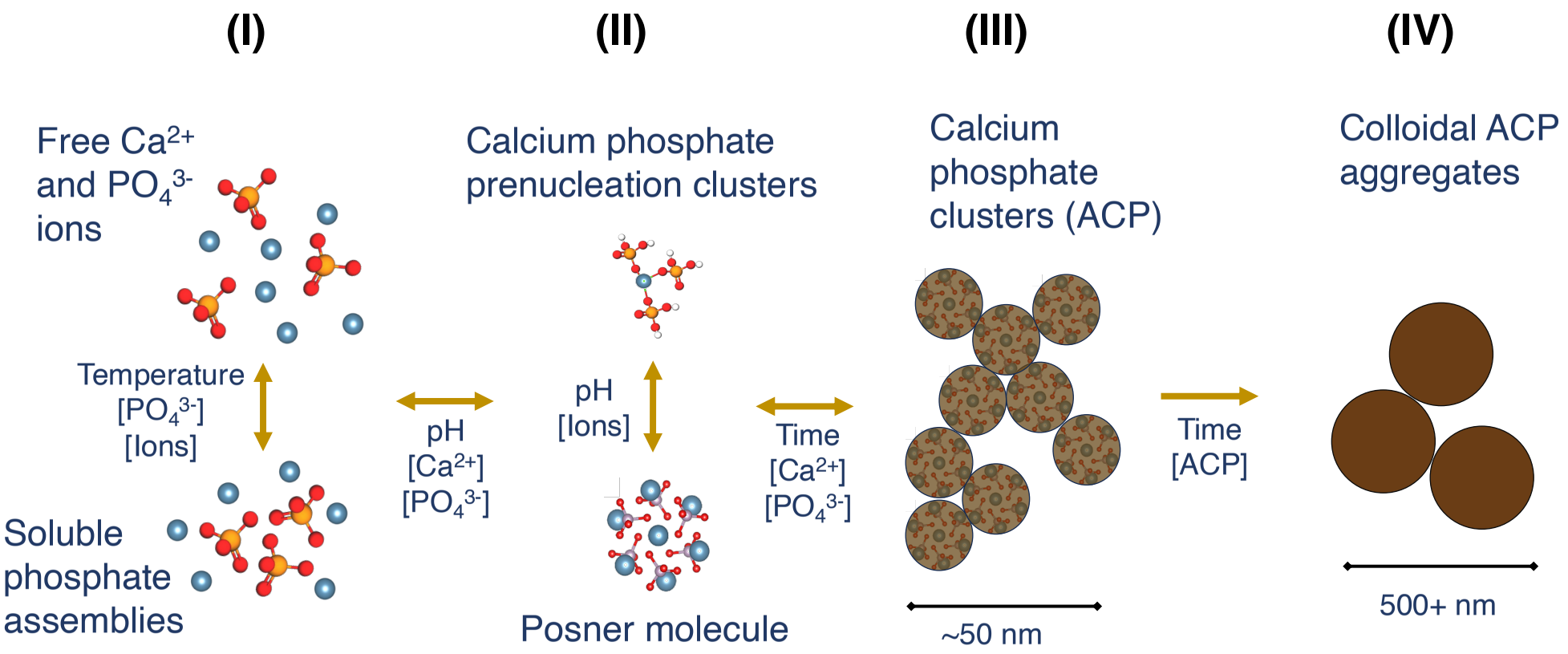
(I)
(II)
(III)
(IV)
Free Ca^{2+} and PO_4^{3-} ions
Temperature
$[PO_4^{3-}]$
[Ions]
Soluble phosphate assemblies
pH
$[Ca^{2+}]$
$[PO_4^{3-}]$
Calcium phosphate prenucleation clusters
pH
[Ions]
Posner molecule
Time
$[Ca^{2+}]$
$[PO_4^{3-}]$
Calcium phosphate clusters (ACP)
~50 nm
Time
[ACP]
Colloidal ACP aggregates
500+ nm

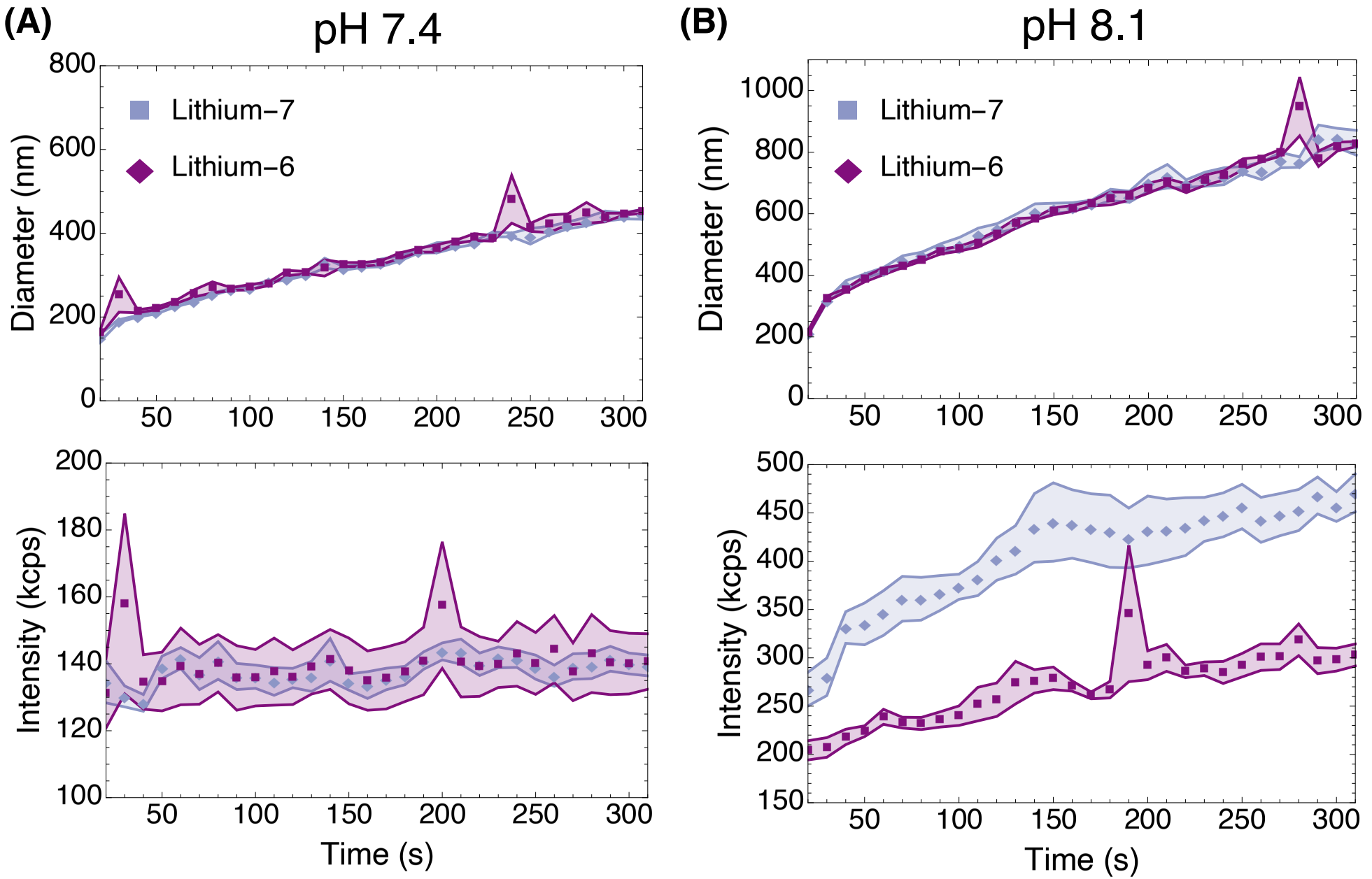
(A)
pH 7.4
Lithium–7
Lithium–6
Diameter (nm)
0
200
400
600
800
50
100
150
200
250
300
Intensity (kcps)
100
120
140
160
180
200
Time (s)
(B)
pH 8.1
Lithium–7
Lithium–6
Diameter (nm)
0
200
400
600
800
1000
Intensity (kcps)
150
200
250
300
350
400
450
500
Time (s)

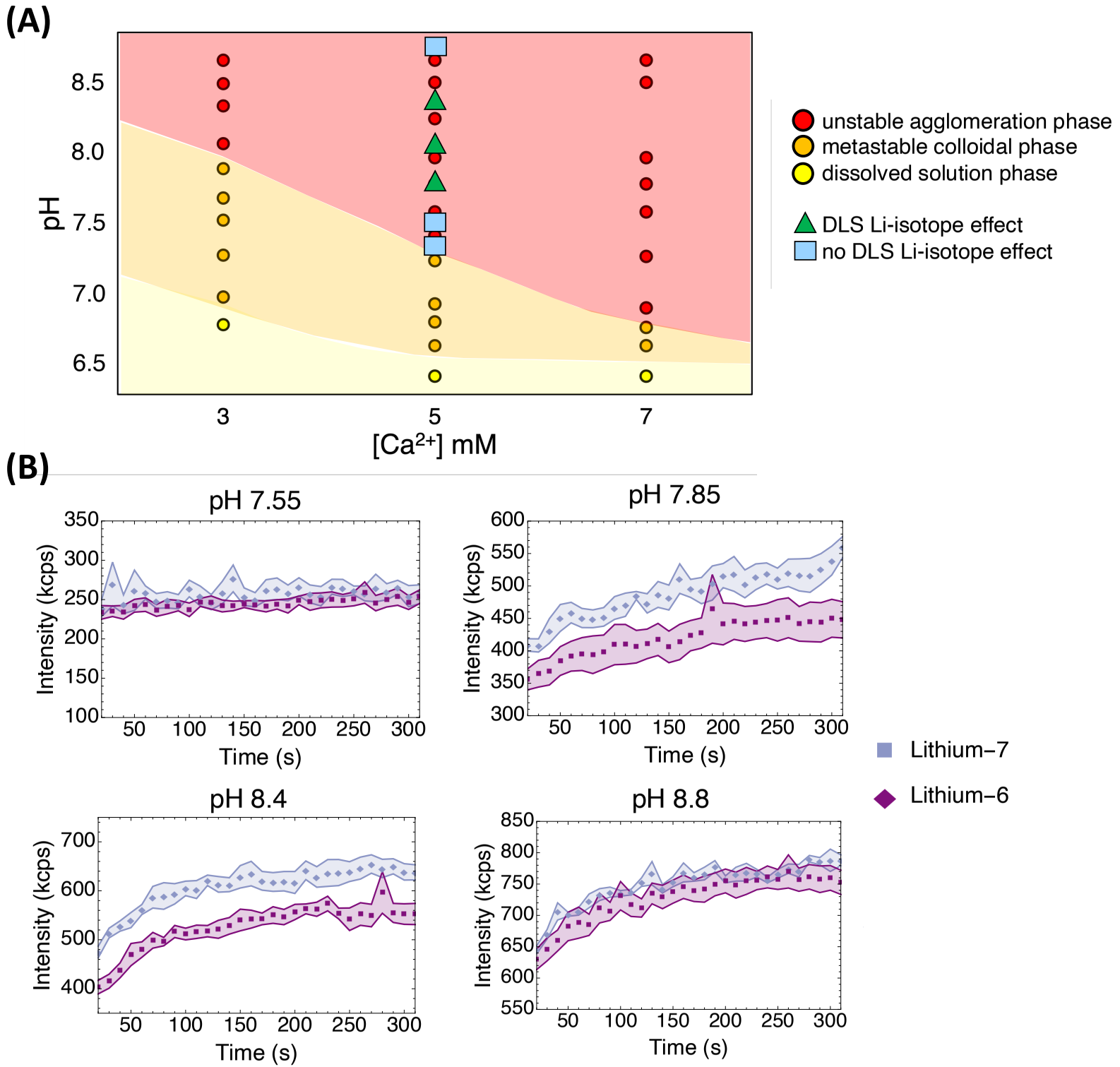
(A)
8.5
8.0
7.5
7.0
6.5
pH
3
5
7
[Ca2+] mM
unstable agglomeration phase
metastable colloidal phase
dissolved solution phase
DLS Li-isotope effect
no DLS Li-isotope effect
(B)
pH 7.55
pH 7.85
pH 8.4
pH 8.8
Intensity (kcps)
Time (s)
Lithium–7
Lithium–6

(A) – ^{31}P solution NMR

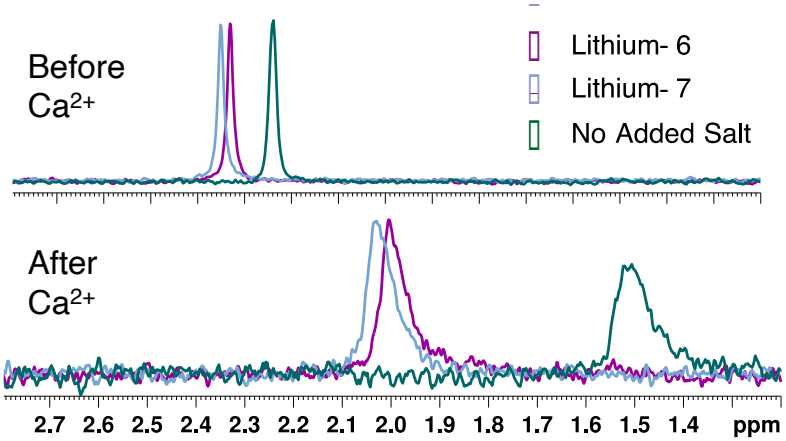

(B) – ICP-MS

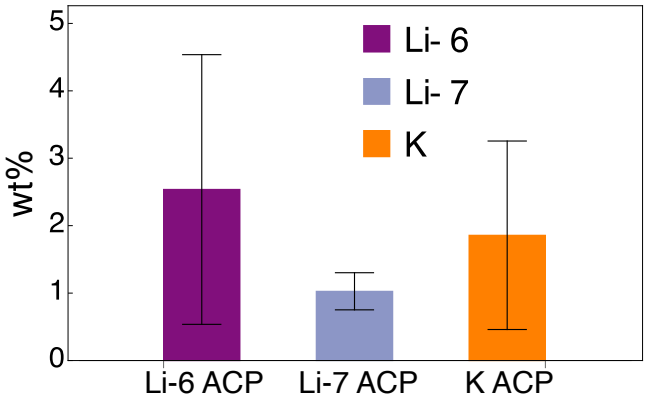

(C) – ^{31}P-^{6}Li REDOR

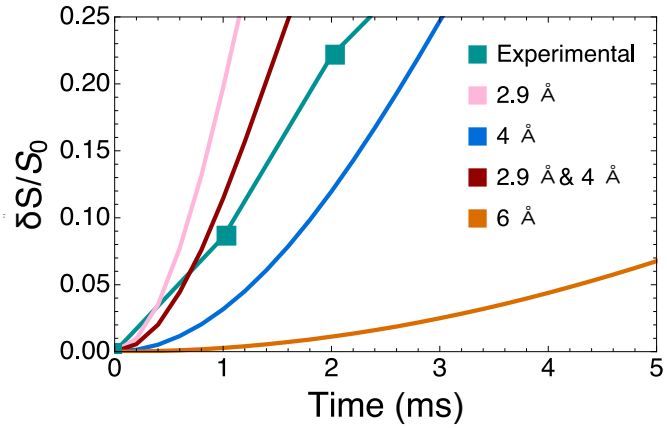

(D) – DFT Li-Posner

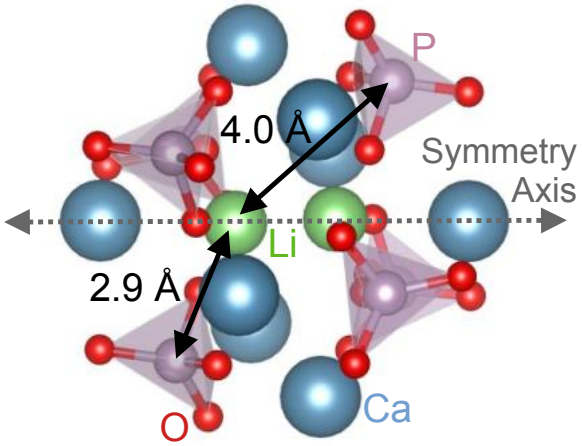

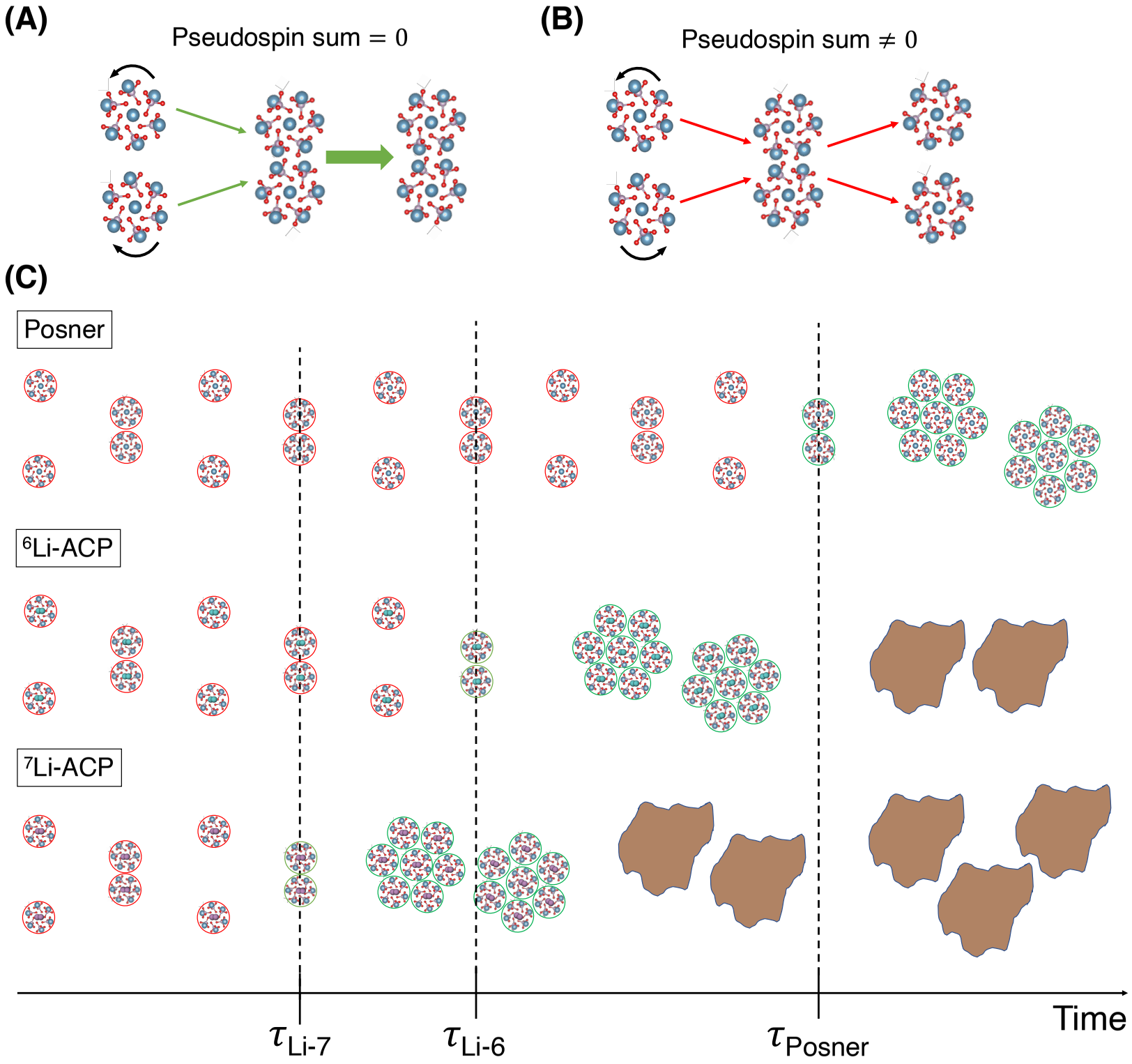
(A)
Pseudospin sum = 0
(B)
Pseudospin sum ≠ 0
(C)
Posner
^{6}Li-ACP
^{7}Li-ACP
$\tau_{\text{Li-7}}$
$\tau_{\text{Li-6}}$
τ_{Posner}
Time

A differential lithium isotope effect on the formation of amorphous calcium phosphate from solution: Supplemental Information

This PDF file includes

MATERIALS AND METHODS

Phosphate stock solutions were made by mixing sodium phosphate tribasic (MW 163.94, Acros Organics, pure) and ortho-phosphoric acid (85%, Fisher Scientific) to reach pH 7. Calcium chloride dihydrate (FW 147.01, 99.7% purity) and potassium chloride (MW 74.55, 99-100.5 % purity) was acquired from Fisher Scientific. Lithium-6 chloride (MW 41.47, 95 atom %) and Lithium-7 chloride (MW 42.47, 99 atom %) were acquired from Sigma Aldrich, and ICP-MS confirmed no significant impurities. Sodium hydroxide (MW 40.00, 99% purity, EMD Millipore) was used to create 0.2 M NaOH solution for pH adjustment. Milli-Q water was used for all solutions.

DLS experiments

Dynamic light scattering was conducted with a BI-200SM Goniometer System with a TurboCorr correlator (Brookhaven Instruments) and a Cobolt Samba 500 mW laser at 532 nm (HÜBNER Photonics). DLS measurements were carried out at a 90° scattering angle with 200 correlation channels ranging from 100 ns to 100 ms and sampling rates of 25 ns, 5 ms, and 50 ms, depending on the channel delay. This experimental setup can be seen in Figure S1.

Solutions were prepared by pH 7 sodium phosphate solution and lithium salt (^{6}LiCl or ^{7}LiCl) in milliQ water, then adjusting pH to desired value with 0.2 M NaOH. Solutions were then filtered with an inline filtration system using a peristaltic pump and a 0.2 μm pore size cellulose acetate filter for 15 minutes. These solutions were then monitored for 120 with DLS to confirm that there were no significant sources of scattering that would indicate contamination which could seed nucleation or affect scattering intensities during ACP formation. The solution pH was measured after filtering and heating to 37 °C to confirm that both lithium solutions were still at the same pH.

Once solutions were prepared, aliquots of 2.85 mL were prepared at 37 °C and 100 mM $CaCl_2$ was heated to 37 °C for at least 10 minutes to allow for equilibration. 150 μL of $CaCl_2$ was then added to the aliquots and after 2 seconds the solutions were vortex mixed for 5 seconds before being inserted into DLS sample cell. Samples were then left to sit for 8 seconds to suppress currents from mixing before data collection began, so that DLS data collection began 15 seconds after calcium addition.

DLS was collected in 10 second increments for 5 minutes at 90° scattering angle at 37° C. The z-average size for each 10 second period was found by fitting using the method of cumulants with a quadratic fit, and the intensity was measured in average counts per second at the detector over each 10 second period.

UV-visible spectroscopy

Optical density traces were monitored using a BioTek Synergy Multimode plate reader, with black clear-bottom 384-well plates. Plates were prepared by first setting up an array of solutions containing 250 mM lithium chloride and 2 mM sodium phosphate. The pH of each solution was adjusted to the desired values, ranging from 6.4 to 8.8, using 0.2 M NaOH. These solutions were then transferred into well plates and heated to 37 °C using an Eppendorf Thermomixer, with 3 replicate wells per solution condition. After temperature equilibration for 15 minutes, calcium chloride was added to each well at appropriate volumes to achieve 3 mM, 5 mM, and 7 mM calcium concentrations, followed by rapid mixing for 5 seconds. Absorbance measurements were carried out at 532 nm wavelength over a period of 35 minutes.

Solid ACP synthesis

For solid ACP synthesis, 500 mLs of solution of 2 mM sodium phosphate and 250 mM lithium chloride or potassium chloride were prepared and brought to pH 7.8. Calcium chloride was then added to bring the final calcium concentration to 5 mM. The solution was then let sit for 5 minutes, to allow for initial nucleation events to mimic the conditions used in DLS. 15 mLs 0.2 M NaOH was then added to each sample to cause ACP to precipite. A Buchner funnel under vacuum with filter paper was used to capture precipitate which was then washed with milliQ water. The resulting ACP paste was removed from the filter paper and lyophilized for 72 hours to form dried powder and stored at -4 °C.

NMR Experiments

Solution NMR relaxation experiments were performed on a Bruker Avance NEO 500 MHz spectrometer with a CryoProbe Prodigy BBO probe, using Wilmad-LabGlass 5 mm Thin Wall

Precision NMR tubes. Solutions were prepared identically to DLS experiments, except with 10% D_2O instead of all milliQ water. 1D ^{31}P spectra were acquired with a 90 degree pulse and 16 scans, with a delay of 10 second between pulses and a 1 second acquisition time at 37 ° C.

Solid state NMR experiments were performed on a Bruker ASCEND DNP-NMR spectrometer (9.4T T) at room temperature and employing a 3.2 mm MAS DNP-NMR triple resonance broad-band X/Y/H probe (Bruker) with ^6Li on the Y channel at 10 kHz MAS. REDOR experiments were executed following pulse sequence protocol from Gullion [1], with cross polarization from ^1H to ^{31}P and power variation on the ^6Li channel. A relaxation delay of 5 s, ^1H pi/2 of 3.92 us at 50 W, ^{31}P pi/2 of 5.3 us at 100 W, and ^6Li pi/2 of 15.2 us at 250 W were used. Distance simulations were completed using SIMPSON 4.1.1. Double quantum and triple quantum filtering, along with spin counting experiments, were completed using the same pulse sequence found in Nowotarski [2].

ICP-MS

ICP-MS experiments were performed with laser ablation on solid powders using the Photon Machines Excite laser and the Agilent 7700X quadrupole ICP-MS. The procedures used followed [3]. Samples were synthesized as described above. ^7Li and ^6Li signals were calibrated using NIST Standard Reference Material 610.

Density Functional Theory Calculations

Density functional theory calculations were implemented as in the VASP code [4, 5]. To achieve accurate energetics, electronic structure, and geometries, we utilize the hybrid functional of Heyd, Scuseria, and Ernzerhof [6]; we use the standard parameterization with a 25% mixing parameter and 0.20 $Å^{-1}$ screening parameter, known as HSE06 [7]. Electron wavefunctions are expanded in a plane-wave basis with an energy cutoff of 500 eV, and the projector augmented wave method is used [8]. The Posner molecule is studied in a vacuum supercell with sides of length 20 Å. We optimize the geometry of the structure until the forces are below 10 meV/Å. To study the effect of Li incorporation, the central Ca^{2+} atom in the Posner molecule is replaced by two Li^+ atoms. We find the Li atoms to be aligned along the diagonal of the Ca cage. Each Li atom is on average 2.89 Å from three P atoms and 4.03 Å from the remaining three P atoms.

REFERENCES

1. T. Gullion, *Concepts in Magnetic Resonance* **10**, 277 (1998).
2. M. Nowotarski, *UC Santa Barbara Theses and Dissertations* (2023).
3. A.R.C. Kylander-Clark, *Reviews in Mineralogy and Geochemistry* **83**, 183 (2017)
4. G. Kresse, J. Furthmüller, *Computational Materials Science* **6**, 15 (1996).
5. G. Kresse, J. Furthmüller, *Physical Review B* **54**, 11169 (1996).
6. J. Heyd, G.E. Scuseria, M. Ernzerhof, *The Journal of Chemical Physics* **118**, 8207 (2003).
7. J. Heyd, G.E. Scuseria, M. Ernzerhof, *The Journal of Chemical Physics* **124**, 219906 (2006).
8. P.E. Blöchl, *Physical Review B* **50**, 17953 (1994).

1. FIGURES AND TABLES

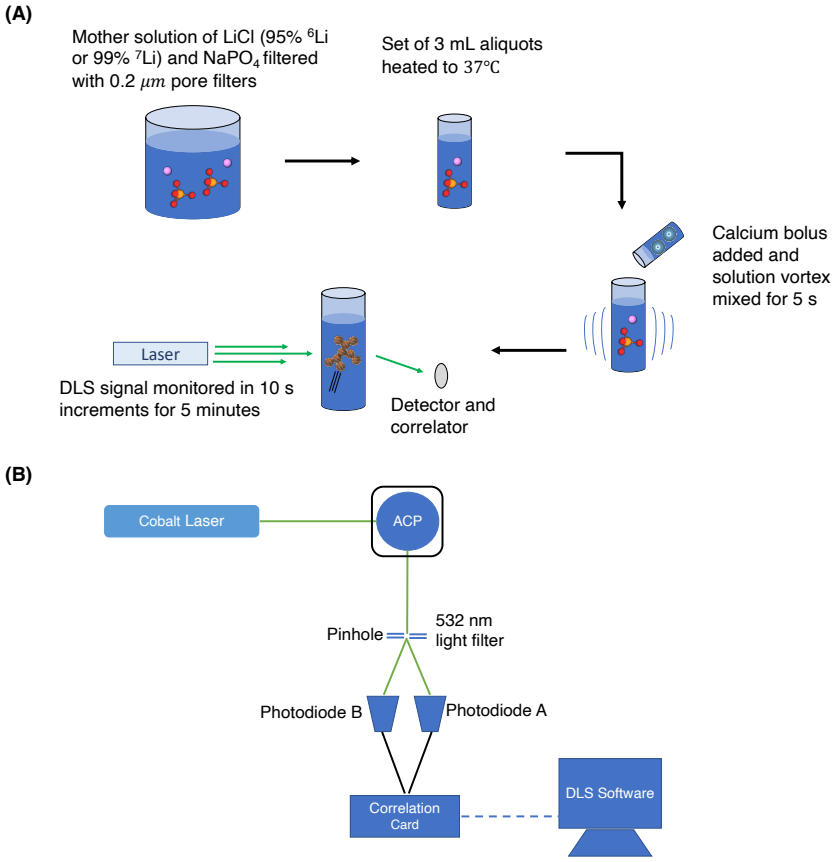

Fig. S1. Protocol and setup for DLS experiments. (A) Solutions of 2mM sodium phosphate and 250 mM lithium chloride were prepared and filtered to remove any contaminants. Aliquots were then heated to 37 °C, before adding calcium chloride (final concentration 5 mM) and rapidly vortex mixing. These solutions were immediately placed into the DLS and monitored for 5 minutes in 10 s blocks. (B) Setup for DLS experiments. Incident 532 nm light is scattered off of the sample and passes through a 532 nm filter. Scattered light then is split into two avalanche photodiodes which are connected to a correlation card that interfaces with DLS software provided by Brookhaven.

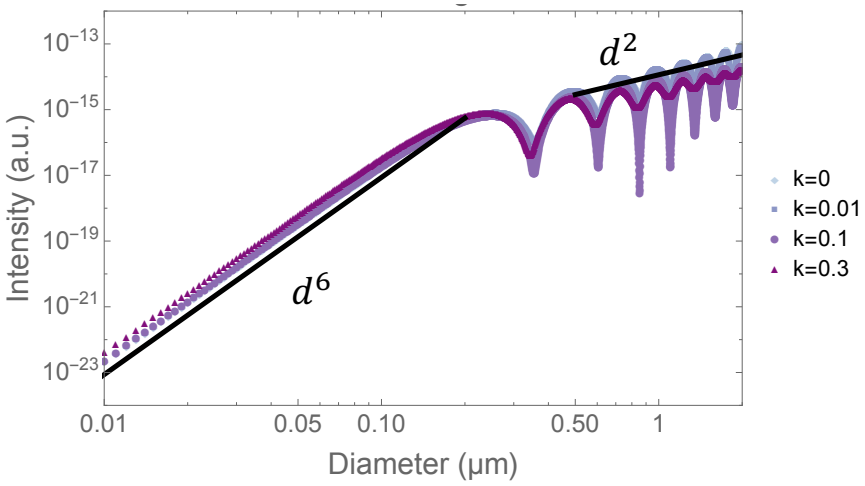

Fig. S2. Scattering intensity vs. diameter for calcium phosphate ($n = 1.626$) for 532 nm light with varying extinction coefficients. Notably, in the Rayleigh regime defined by diameter $d << \lambda$, we see that intensity I scales as $I \propto d^6$, while for sizes greater than the Rayleigh regime we have $I \propto d^2$.

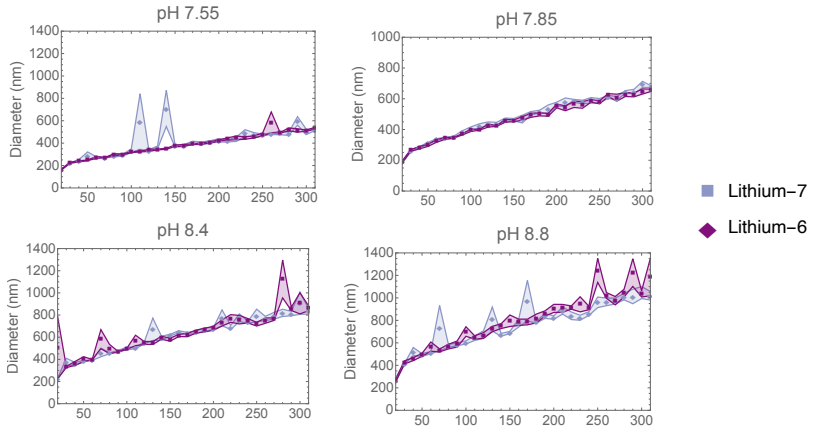

Fig. S3. DLS average diameter time series data at varying pH for samples whose intensity are shown in Figure 3B. Average diameters show no lithium isotope dependence, indicating that the observed intensity difference in Figure 3B is related to particle abundance.

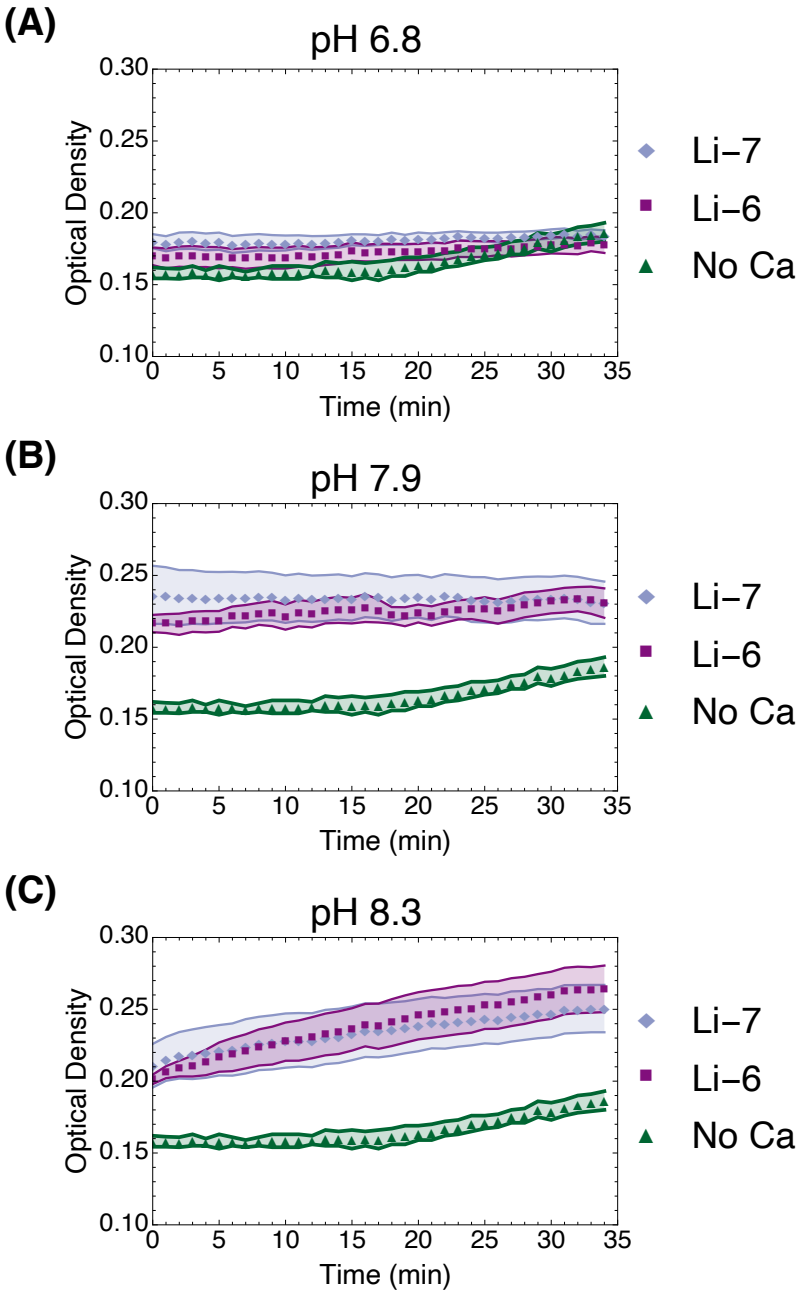

Fig. S4. 35-minute absorbance measurements at 532 nm wavelength identify three distinct stages of calcium phosphate growth in solution phase space. A) At lower pH, solutions are indistinguishable from no-Ca control, corresponding to dissolved free ion phase. B) At intermediate pH, solutions form metastable ACP colloids with constant absorbance traces. C) At higher pH, solutions immediately undergo agglomeration, indicated by steadily increasing absorbance. Note that solutions containing Li-6 or Li-7 exhibit identical absorbance traces.

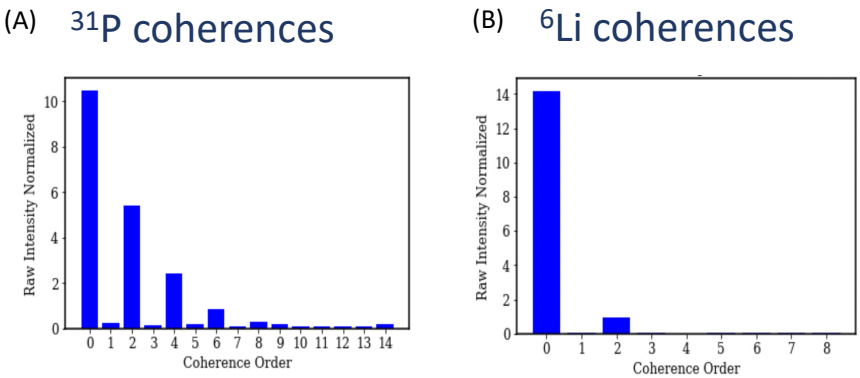

Fig. S5. Spin counting results on ^{6}Li-ACP sample from ICP-MS. (A) ^{31}P spin counting result confirms shows the same coherence orders as ACP, confirming that the phase of the powder. (B) ^{6}Li spin counting results show no coherences order over 2, suggesting there are no large clumps of reprecipitated ^{6}Li in solution that would contribute to the ICP-MS ^{6}Li signal.